

Observation of the superconducting proximity effect from surface states in SmB_6/YB_6 thin film heterostructures via terahertz spectroscopy

Jonathan Stensberg,¹ Xingyue Han,¹ Seunghun Lee,^{2,3} Stephen A. McGill,⁴
Johnpierre Paglione,⁵ Ichiro Takeuchi,^{2,5} Charles L. Kane,¹ and Liang Wu^{1,*}

¹*Department of Physics and Astronomy, University of Pennsylvania, Philadelphia, Pennsylvania 19104, U.S.A*

²*Department of Materials Science and Engineering,
University of Maryland, College Park, MD 20742, USA.*

³*Department of Physics, Pukyong National University, Busan 48513, Republic of Korea*

⁴*National High Magnetic Field Laboratory, FSU, Tallahassee, Florida 32310, USA*

⁵*Maryland Quantum Materials Center, University of Maryland, College Park, MD 20742, USA.*

(Dated: January 27, 2023)

The AC conduction of epitaxially-grown SmB_6 thin films and superconducting heterostructures of SmB_6/YB_6 are investigated via time domain terahertz spectroscopy. A two-channel model of thickness-dependent bulk states and thickness-independent surface states accurately describes the measured conductance of bare SmB_6 thin films, demonstrating the presence of surface states in SmB_6 . While the observed reductions in the simultaneously-measured superconducting gap, transition temperature, and superfluid density of SmB_6/YB_6 heterostructures relative to bare YB_6 indicate the penetration of proximity-induced superconductivity into the SmB_6 overlayer; the corresponding SmB_6 -thickness independence between different heterostructures indicates that the induced superconductivity is predominantly confined to the interface surface state of the SmB_6 . This study demonstrates the ability of terahertz spectroscopy to probe proximity-induced superconductivity at an interface buried within a heterostructure, and our results show that SmB_6 behaves as a predominantly insulating bulk surrounded by conducting surface states in both the normal and induced-superconducting states in both terahertz and DC responses, which is consistent with the topological Kondo insulator picture.

Introduction

SmB_6 has long been identified as a mixed-valence Kondo insulator with an anomalous low-temperature resistance plateau that eluded explanation [1–4]. Following the discovery of topological insulators [5–8], it was proposed that this anomalous resistance plateau is due to topologically protected surface states, making SmB_6 the first topological Kondo insulator (TKI) [9–12]. Following this prediction, a flurry of experiments have investigated the basic features of such a TKI [13–29], yet despite the evidence in support of the TKI prediction, controversy has continued to surround SmB_6 [30–42]. Much recent work has therefore been dedicated to understanding experimental discrepancies and harmonizing results. Numerous studies have now highlighted common extrinsic issues with studies of bulk crystals, including subsurface cracks in polished bulk samples [41], aluminum inclusions in crystals grown by the aluminum flux method [43], residual bulk conduction attributed to one dimensional crystalline dislocations [41, 44–46], and localized metallic islands around sample impurities [47, 48]. Furthermore, previous terahertz studies [49, 50] of SmB_6 starkly diverged from DC transport by finding an anomalously large AC conductivity without evidence for surface states. These results created a confused picture of SmB_6 with radically different AC and DC behaviors that has been frequently invoked by both experimental and theoretical efforts [34, 36, 45, 48]. However, these terahertz

studies were performed using polished bulk crystals that may suffer from the confounding effects mentioned previously and may therefore be reporting extrinsic behaviors.

Whereas most experiments on SmB_6 have employed bulk crystals, it has recently become possible to grow high-quality epitaxial thin films of SmB_6 via sputtering [21, 51, 52], thereby avoiding the myriad extrinsic concerns with bulk crystals and circumventing issues [53] in comparing previous results achieved via the different bulk crystal growth methods. By forming thin film heterostructures of SmB_6 with the isostructural BCS superconductor YB_6 , perfect Andreev reflection has been observed at the surface of sufficiently-thin SmB_6 overlayers via point contact Andreev reflection (PCAR) spectroscopy [51]. These results indicate the presence of metallic surface states susceptible to the superconducting proximity effect in these epitaxially grown SmB_6 samples and, moreover, indicate that these surface states are indeed topologically protected in accord with the TKI prediction. Such heterostructures are predicted to host topological superconducting states at the buried interface [8, 54] and could be engineered to generate and manipulate Majorana modes to perform topological quantum computations [8, 54]. However, such buried interface states are not accessible by standard surface probes such as angle resolved photoemission spectroscopy (ARPES), scanning tunneling spectroscopy/microscopy (STS/M), or PCAR spectroscopy.

Here, we perform time-domain terahertz spectroscopy (TDTS) on epitaxially grown thin films of SmB_6 and SmB_6/YB_6 heterostructures. We find an AC conductiv-

* liangwu@sas.upenn.edu

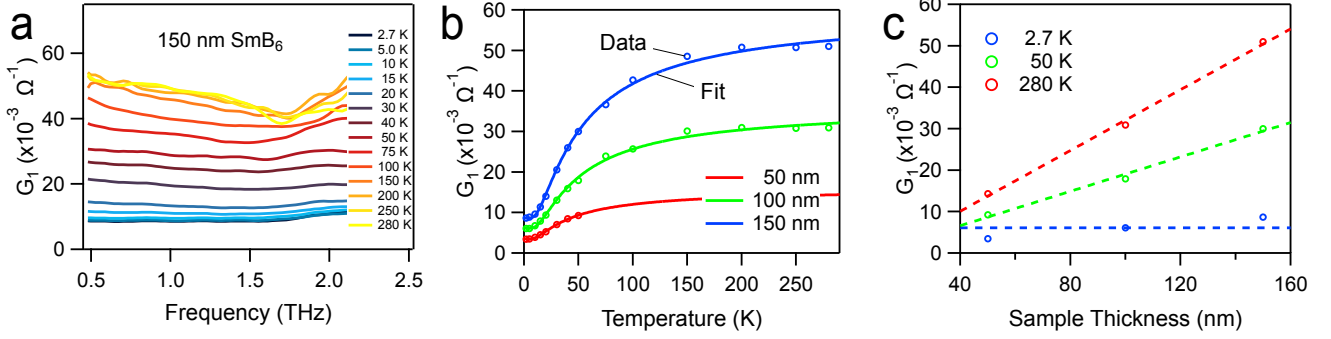


FIG. 1. **a.** The real part of the complex conductance of a 150 nm epitaxial thin film of SmB_6 from 2.7 K to 280 K. Complete data for all three samples is provided in Fig. S2 of the SI. **b.** The average conductance over 0.5-1.0 THz for each SmB_6 sample fitted by the two channel conductance model across the temperature range. **c.** Thickness dependence of the average conductance at various temperatures for each SmB_6 sample. The thickness dependence of all temperatures is provided in Fig. S4 of the SI.

ity in harmony with DC transport results, demonstrating strong evidence for the presence of surface states in SmB_6 at low temperatures and the confinement of the superconducting proximity effect to the surface state at the interface of the SmB_6/YB_6 heterostructures. Altogether, we establish a straightforward and unified understanding of the intrinsic low temperature conductance of SmB_6 : in both the normal and induced-superconducting states, SmB_6 behaves as a predominantly insulating bulk surrounded by conducting surface states in both AC and DC, as expected under the TKI prediction.

Results and Discussion

Thin film samples of SmB_6 are grown epitaxially on Si (001) substrates via sputtering [51]. In order to form a minimal-barrier interface with SmB_6 , the isostructural BCS superconductor YB_6 is selected for the proximity effect heterostructures. As the superconducting transition temperature T_C of YB_6 is maximized in the case of mild boron deficiency [51], 100 nm layers of $\text{YB}_{5.6}$ are grown on Si (001) substrates via sputtering, which for convenience will be referred to as YB_6 throughout. Heterostructures of SmB_6/YB_6 are fabricated by growing a 20 nm or 100 nm SmB_6 overlayer sequentially atop 100 nm YB_6 samples *in situ* without breaking vacuum in the sputtering chamber [51].

Typical TDTS [55] data for the real conductance G_1 is shown for the 150 nm SmB_6 sample in Fig. 1.a (Raw TDTS time trace data is provided in Fig. S1 of the supplementary information (SI)). There are no pronounced spectral features across the reliable frequency range of ~ 0.5 -2.3 THz, though there is a mild Drude-like conductivity that decreases in prominence at lower temperatures. Notably, the conductance of the sample plateaus below 5 K across the entire spectral range. In order to compare the conductance between samples, the average of the spectrum is taken from 0.5 THz to 1.0 THz and shown in Fig. 1.c for select temperatures (See Fig. S4.a of the SI for all temperatures.). At both 50 K and 280 K, the conductance increases linearly with sample thick-

ness, consistent with bulk-dominated behavior, whereas the conductance is nearly independent of sample thickness at 2.7 K, consistent with surface-dominated behavior. The small amount of thickness dependence that remains at low temperature may be due in part to the limited number of samples available for study, but may also result from a small residual bulk conductivity.

To assess the conductance across the temperature range and available sample thicknesses, we apply a two-channel model of the total conductance G_{tot} [15, 21]. One channel scales with thickness and is exponentially activated as a function of temperature, consistent with a bulk conductance G_{bulk} . The second is a temperature- and thickness-independent channel consistent with a surface conductance G_{surf} resulting from both the upper and lower surface states. The two-channel model is thus given by

$$G_{tot}(T) = G_{surf} + G_{bulk}(T) \quad (1)$$

$$G_{surf} = G_{LT} \quad (2)$$

$$G_{bulk}(T) = \sigma_{bulk,HT} t_{bulk} \exp\left(\frac{E_a}{k_B T_{HT}} - \frac{E_a}{k_B T}\right) \quad (3)$$

where G_{LT} is the conductance at low temperature, $\sigma_{bulk,HT}$ is the bulk conductivity at high temperature, t_{bulk} is the thickness of the bulk conductance channel, E_a is the characteristic activation energy of the bulk channel, k_B is the Boltzmann constant, and T_{HT} is the temperature at which the high temperature conductivity is calculated. Since the measured low temperature conductance is reasonably consistent across the thin films, in contrast to bulk samples where it can vary by orders of magnitude [41, 46], Equations 1-3 can be fit to the data while extracting the conductance of each channel, the thickness of each channel, and the bulk activation energy. As can be seen in Fig. 1.b, the two channel conductance model

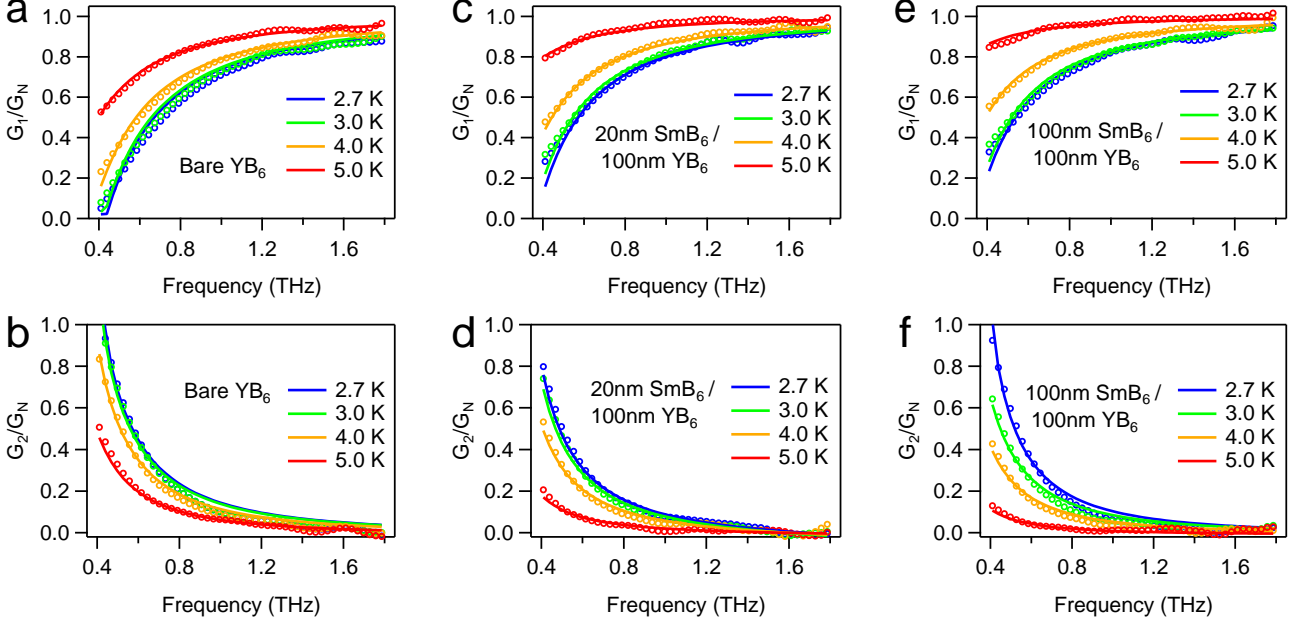


FIG. 2. Normalized real and imaginary parts, respectively, of the complex conductance in the superconducting state for bare 100 nm YB₆ (a,b), 20 nm SmB₆ / 100 nm YB₆ (c,d), and 100 nm SmB₆ / 100 nm YB₆ (e,f). The real and imaginary parts of the data for each sample, given by the circles, are simultaneously fit to produce the solid lines. Unnormalized data for all heterostructures is provided in Fig. S3 of the SI.

provides a strong fit to the data for the three samples (experimental data above 50 K for the 50 nm sample proved unreliable possibly due to the substrates being from different batches). The average fitted value of the bulk activation energy $E_a = 3.8$ meV is consistent with the range of results from previous DC transport measurements on bulk SmB₆ crystals [14, 15, 18, 21, 22, 44, 45, 47]. The fitted values for the thickness of the bulk conductance channel increase linearly with sample thickness in a near one-to-one ratio, indicating the change in conductance between samples is overwhelmingly due to the different thickness of the bulk conducting channel. By considering the actual sample thickness $d = t_{\text{bulk}} + 2t_{\text{surf}}$, the effective thickness of the surface channel t_{surf} is determined to be consistent and non-negligible, with an average value of $t_{\text{surf}} = 9.1$ nm consistent with previous reports [21, 52]. This provides strong evidence for surface conducting states in bare SmB₆ at low temperature and resolves the previous discrepancy between AC and DC conductance in SmB₆.

Superconducting heterostructures of SmB₆/YB₆ are probed via the same TDTS method and compared to a thin film sample of YB₆ ($T_C \approx 6.1$ K) with no overlayer of SmB₆. As all samples consist of 100 nm YB₆ and some thickness of SmB₆, each heterostructure is referred to by its SmB₆ thickness for convenience. Typical data for the bare YB₆, the 20 nm heterostructure, and the 100 nm heterostructure are shown in Fig. 2.a,b; Fig. 2.c,d; and Fig. 2.e,f, respectively, where the superconducting low temperature conductance $\hat{G} = G_1 + iG_2$ is

normalized by the normal state conductance G_N of the sample above T_C at 10 K. Conductance data of this form is modeled by the Mattis-Bardeen formalism for the optical response of a BCS superconductor in the dirty limit below T_C as the superconducting gap opens [56, 57]. See SI for extended fitting details.

By simultaneously fitting the real and imaginary parts of the normalized conductance for a sample at a given temperature T , the superconducting gap $\Delta(T)$ at that temperature can be extracted for a given guess value of T_C . By taking an initial estimate of T_C from the disappearance of superconducting behavior in the terahertz spectrum and repeating the simultaneous fitting for each temperature, as shown by the solid lines in Fig. 2, the temperature evolution of $\Delta(T)$ is extracted. For a BCS superconductor, this temperature evolution is approximated by [58]

$$\Delta(T) \approx \Delta_0 \tanh(1.74\sqrt{T_C/T - 1}) \quad (4)$$

By fitting Δ_0 and T_C to the extracted values of $\Delta(T)$, the guess value of T_C can be updated. Thus by iteratively performing the simultaneous Mattis-Bardeen fitting and BCS gap fitting until convergence, values of Δ_0 and T_C for each sample are extracted from the data. As Δ_0 varies on both sides of the interface of proximity-effect heterostructures [59, 60], the measured values of Δ_0 are effective averages for the heterostructure.

This iterative method results in a high-quality fit, as shown in Fig. 2 and Fig. 3.a, with all samples following the BCS behavior. The clear reduction in both T_C

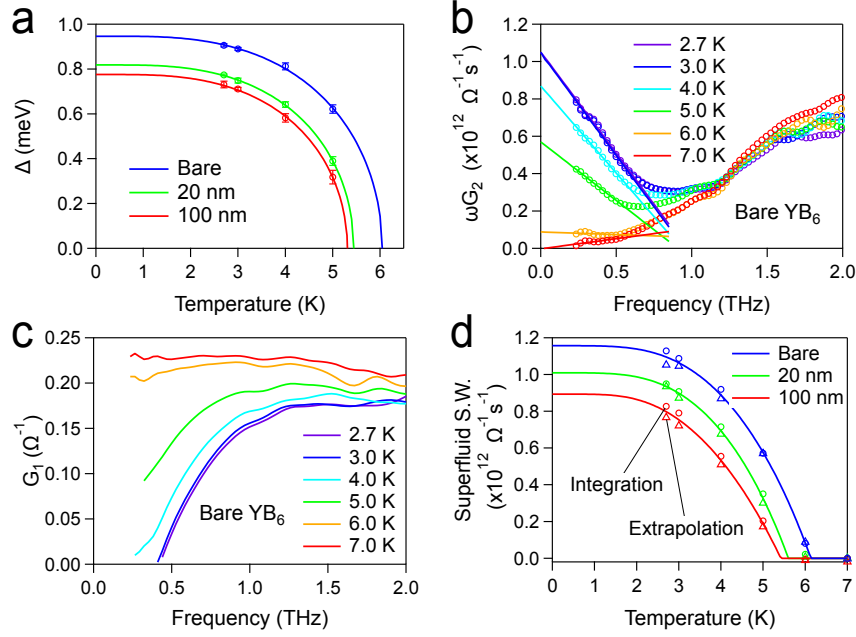


FIG. 3. **a.** BCS fitting of the temperature dependence of the superconducting gap data, $\Delta(T)$, extracted from the Mattis-Bardeen fitting for each superconducting sample. Error bars are determined by the Mattis-Bardeen fitting. **b.** The linear portion of ωG_2 shown for bare 100 nm YB₆ is fitted to permit measurement of the superfluid spectral weight by extrapolation of the fit down to zero frequency. **c.** The difference in G_1 shown for bare 100 nm YB₆ is integrated out to 2.0 THz, where the conductance has started to converge, to measure the superfluid spectral weight via integration. **d.** The superfluid spectral weight determined by the extrapolation and integration methods for each superconducting sample are simultaneously fit by the expected temperature dependence. Error bars for the extrapolation method are smaller than the markers.

and Δ_0 from the bare YB₆ to the heterostructures indicates that superconductivity is being induced in some portion of the SmB₆ overlayer via the superconducting proximity effect. For an ordinary metallic overlayer, the reduction in T_C and Δ_0 due to the proximity effect depends strongly on the thickness of the metallic layer for thin films, where the sample thickness is on the order of the normal coherence length, or less [59, 60]. However, the reductions observed in the heterostructures here vary only slightly despite the thickness of the SmB₆ considerably spanning the normal coherence length, which was previously determined to be ~ 50 nm [52]. The weak SmB₆-thickness dependence of the measured T_C and Δ_0 suggests that the effective thickness of the SmB₆ that is metallic and susceptible to the proximity effect is largely independent of the actual thickness of the SmB₆ overlayer, contrary to the expectation for sample thicknesses on the order of the normal coherence length. This result therefore implies that the dominant contribution to the conductivity is restricted to the surface state at the interface, and that the bulk SmB₆ is only weakly conducting at best. Thus the observed weak SmB₆-thickness dependence of T_C and Δ_0 in the superconducting heterostructures concurs with the model of SmB₆ as consisting of metallic surface states surrounding an insulating bulk.

The measurement of the complex conductance in the superconducting heterostructures also affords a measure-

ment of the superfluid spectral weight, indicating the temperature evolution of the superfluid density in the samples. The superfluid spectral weight can be extracted by two methods, which we will call the extrapolation and integration methods. The extrapolation method makes use of the fact that the superfluid spectral weight is given by [61]

$$S_{extr}(T) = \lim_{\omega \rightarrow 0} \omega G_2^{SC}(\omega, T) \quad (5)$$

where G_2^{SC} is the imaginary conductivity in the superconducting state. Extracting values of S_{extr} for each temperature is accomplished by fitting to the linear portion of $\omega G_2(\omega, T)$, as shown in Fig. 3.b, and extrapolating to zero frequency. The integration method directly calculates the loss of spectral weight when passing below T_C according to [61]

$$S_{int}(T) = \int_0^\infty d\omega (G_1^N(\omega) - G_1^{SC}(\omega, T)) \quad (6)$$

where $G_1^N(\omega)$ and $G_1^{SC}(\omega, T)$ are the real conductivity in the normal state and superconducting states, respectively. Given the convergence of G_1 at high frequency, the upper limit of integration can be reasonably truncated to the limit of reliable data, as shown in Fig. 3.c, introducing only minor error. Fig. 3.d shows that while the integration method consistently yields a slightly larger

value for the superfluid spectral weight, the two methods show reasonable agreement across the temperature range for each sample. The temperature dependence of the superfluid spectral weight is given by [58, 61]

$$S(T) = S(0) \frac{\Delta(T)}{\Delta_0} \tanh\left(\frac{\Delta(T)}{2k_B T}\right) \quad (7)$$

Simultaneous fits of the data for both the extrapolation and integration methods are shown in Fig. 3.d, showing strong agreement across the temperature range. There is a clear decrease in the superfluid spectral weight between each sample. The decrease from bare YB₆ to the heterostructure is expected as a result of the superconducting proximity effect. However, whereas Δ_0 is quite comparable between the heterostructures and shows a difference of just 5 percent, $S(0)$ shows a more significant decrease of 12 percent. The minimal difference in Δ_0 indicates that the proximity effect is predominantly confined to the same volume in both heterostructures, namely the surface states as identified above. The further reduction in $S(0)$ with increased SmB₆ thickness, however, may be attributable to very weak conducting states existing in the bulk [41, 44–46]. As the superfluid spectral weight is not yet thoroughly explored in the literature, further work is warranted to understand the significance of this behavior.

To summarize, these results provide a simple and unified picture in concord with the TKI prediction: SmB₆ behaves as a predominantly insulating bulk surrounded by conducting surface states in both the normal and induced-superconducting states in both AC and DC conduction. Experimental explanations and theoretical speculations that invoked the previous anomalous AC response may need to be reconsidered in light of these findings. While a topologically trivial explanation for this behavior cannot be ruled out by measurements presented

here, the previous observation of perfect Andreev reflection [51] in similar SmB₆/YB₆ heterostructures supports the topological origin.

Furthermore, the measurements presented here demonstrate that TDTS can provide an effective probe of superconducting states at the buried interface of these important superconductor-topological insulator heterostructures, providing a powerful new tool for the investigation of engineered topological superconducting systems. Looking forward, our methods can extend to other topological superconducting heterostructures with bulk-insulating topological insulators such as Bi₂Se₃[62–64] and Sb₂Te₃[65] where the proximity effect does not reach the sample surface yet remains active in the buried interface.

Acknowledgement

We thank P. Chauhan for helpful discussions. This project is mainly supported by L.W.’s startup package at the University of Pennsylvania. J.S. and X.H. are partially supported by the ARO under the Grants W911NF1910342 and W911NF2020166, and the Gordon and Betty Moore Foundation’s EPiQS Initiative, Grant GBMF9212 to L.W. The acquisition of the laser for the THz system is supported from a seed grant at the National Science Foundation supported University of Pennsylvania Materials Research Science and Engineering Center (MRSEC)(DMR-1720530). J.S. is also partially supported by the NSF EAGER grant via the CMMT program (DMR-2132591). C.L.K is supported by a Simons Investigator grant from the Simons Foundation. S.L., J.P., and I.T. are supported by AFOSR FA9550-14-1-0332. L.W. acknowledges support from the NHMFL Visiting Scientist Program and partial summer support from the NSF EAGER grant.

-
- [1] A. Menth, E. Buehler, and T. H. Geballe, Magnetic and Semiconducting Properties of SmB₆, *Phys. Rev. Lett.* **22**, 295 (1969).
 - [2] J. C. Nickerson, R. M. White, K. N. Lee, R. Bachmann, T. H. Geballe, and G. W. Hull, Physical Properties of SmB₆, *Phys. Rev. B* **3**, 2030 (1971).
 - [3] N. Mott, Rare-earth compounds with mixed-valencies, *Philos. Mag.* **30** (1974).
 - [4] C. M. Varma, Mixed-valence compounds, *Rev. Mod. Phys.* **48**, 219 (1976).
 - [5] C. L. Kane and E. J. Mele, Z₂ Topological Order and the Quantum Spin Hall Effect, *Phys. Rev. Lett.* **95**, 146802 (2005).
 - [6] C. L. Kane and E. J. Mele, Quantum Spin Hall Effect in Graphene, *Phys. Rev. Lett.* **95**, 226801 (2005).
 - [7] L. Fu, C. L. Kane, and E. J. Mele, Topological Insulators in Three Dimensions, *Phys. Rev. Lett.* **98**, 106803 (2007).
 - [8] M. Z. Hasan and C. L. Kane, Colloquium: Topological insulators, *Rev. Mod. Phys.* **82**, 3045 (2010).
 - [9] M. Dzero, K. Sun, V. Galitski, and P. Coleman, Topological Kondo Insulators, *Phys. Rev. Lett.* **104**, 106408 (2010).
 - [10] T. Takimoto, SmB₆: A Promising Candidate for a Topological Insulator, *J. Phys. Soc. Jpn.* **80**, 123710 (2011).
 - [11] M. Dzero, K. Sun, P. Coleman, and V. Galitski, Theory of topological Kondo insulators, *Phys. Rev. B* **85**, 045130 (2012).
 - [12] V. Alexandrov, M. Dzero, and P. Coleman, Cubic Topological Kondo Insulators, *Phys. Rev. Lett.* **111**, 226403 (2013).
 - [13] X. Zhang, N. P. Butch, P. Syers, S. Ziemak, R. L. Greene, and J. Paglione, Hybridization, Inter-Ion Correlation, and Surface States in the Kondo Insulator SmB₆, *Phys. Rev. X* **3**, 011011 (2013).
 - [14] D. Kim, S. Thomas, T. Grant, J. Botimer, Z. Fisk, and J. Xia, Surface Hall Effect and Nonlocal Transport in SmB₆: Evidence for Surface Conduction, *Sci. Rep.* **3**, 3150 (2013).

- [15] S. Wolgast, C. Kurdak, K. Sun, J. W. Allen, D.-J. Kim, and Z. Fisk, Low-temperature surface conduction in the Kondo insulator SmB_6 , *Phys. Rev. B* **88**, 180405 (2013).
- [16] D. Kim, J. Xia, and Z. Fisk, Topological surface state in the Kondo insulator samarium hexaboride, *Nature Mater.* **13**, 466–470 (2014).
- [17] W. A. Phelan, S. M. Koohpayeh, P. Cottingham, J. W. Freeland, J. C. Leiner, C. L. Broholm, and T. M. McQueen, Correlation between Bulk Thermodynamic Measurements and the Low-Temperature-Resistance Plateau in SmB_6 , *Phys. Rev. X* **4**, 031012 (2014).
- [18] P. Syers, D. Kim, M. S. Fuhrer, and J. Paglione, Tuning Bulk and Surface Conduction in the Proposed Topological Kondo Insulator SmB_6 , *Phys. Rev. Lett.* **114**, 096601 (2015).
- [19] F. Chen, C. Shang, Z. Jin, D. Zhao, Y. P. Wu, Z. J. Xiang, Z. C. Xia, A. F. Wang, X. G. Luo, T. Wu, and X. H. Chen, Magnetoresistance evidence of a surface state and a field-dependent insulating state in the Kondo insulator SmB_6 , *Phys. Rev. B* **91**, 205133 (2015).
- [20] Y. Nakajima, P. Syers, X. Wang, R. Wang, and J. Paglione, One-dimensional edge state transport in a topological Kondo insulator, *Nature Phys.* **12**, 213 (2016).
- [21] S. Lee, X. Zhang, Y. Liang, S. W. Fackler, J. Yong, X. Wang, J. Paglione, R. L. Greene, and I. Takeuchi, Observation of the Superconducting Proximity Effect in the Surface State of SmB_6 Thin Films, *Phys. Rev. X* **6**, 031031 (2016).
- [22] A. Stern, M. Dzero, V. M. Galitski, Z. Fisk, and J. Xia, Surface-dominated conduction up to 240 K in the Kondo insulator SmB_6 under strain, *Nature Mater.* **16**, 708 (2017).
- [23] M. Neupane, N. Alidoust, S. Xu, T. Kondo, Y. Ishida, D.-J. Kim, C. Liu, I. Belopolski, Y. Jo, T.-R. Chang, *et al.*, Surface electronic structure of the topological Kondo-insulator candidate correlated electron system SmB_6 , *Nature Comm.* **4**, 1 (2013).
- [24] J. Jiang, S. Li, T. Zhang, Z. Sun, F. Chen, Z. Ye, M. Xu, Q. Ge, S. Tan, X. Niu, M. Xia, B. Xie, Y. Li, X. Chen, H. Wen, and D. Feng, Observation of possible topological in-gap surface states in the Kondo insulator SmB_6 by photoemission, *Nature Comm.* **4**, 3010 (2013).
- [25] E. Frantzeskakis, N. de Jong, B. Zwartsenberg, Y. K. Huang, Y. Pan, X. Zhang, J. X. Zhang, F. X. Zhang, L. H. Bao, O. Tegus, A. Varykhalov, A. de Visser, and M. S. Golden, Kondo Hybridization and the Origin of Metallic States at the (001) Surface of SmB_6 , *Phys. Rev. X* **3**, 041024 (2013).
- [26] N. Xu, C. E. Matt, E. Pomjakushina, X. Shi, R. S. Dhaka, N. C. Plumb, M. Radovic, P. K. Biswas, D. Evtushinsky, V. Zabolotnyy, J. H. Dil, K. Conder, J. Mesot, H. Ding, and M. Shi, Exotic Kondo crossover in a wide temperature region in the topological Kondo insulator SmB_6 revealed by high-resolution ARPES, *Phys. Rev. B* **90**, 085148 (2014).
- [27] H. Pirie, Y. Liu, A. Soumyanarayanan, P. Chen, Y. He, M. Yee, P. Rosa, J. Thompson, D.-J. Kim, Z. Fisk, X. Wang, J. Paglione, D. Morr, M. Hamidian, and J. Hoffman, Imaging emergent heavy Dirac fermions of a topological Kondo insulator, *Nature Phys.* **16**, 52 (2020).
- [28] Y. Ohtsubo, Y. Yamashita, K. Hagiwara, S. i. Ideta, K. Tanaka, R. Yukawa, K. Horiba, H. Kumigashira, K. Miyamoto, T. Okuda, W. Hirano, F. Iga, and S. i. Kimura, Non-trivial surface states of samarium hexaboride at the (111) surface, *Nature Comm.* **10**, 2298 (2019).
- [29] N. Xu, P. Biswas, J. Dil, R. Dhaka, G. Landolt, S. Muff, C. Matt, X. Shi, N. Plumb, M. Radovic, E. Pomjakushina, K. Conder, A. Amato, S. Borisenko, R. Yu, H.-M. Weng, Z. Fang, X. Dai, J. Mesot, H. Ding, and M. Shi, Direct observation of the spin texture in SmB_6 as evidence of the topological Kondo insulator, *Nature Comm.* **5**, 4566 (2014).
- [30] O. Erten, P. Ghaemi, and P. Coleman, Kondo Breakdown and Quantum Oscillations in SmB_6 , *Phys. Rev. Lett.* **116**, 046403 (2016).
- [31] G. Li, Z. Xiang, F. Yu, T. Asaba, B. Lawson, P. Cai, C. Tinsman, A. Berkley, S. Wolgast, Y. S. Eo, D.-J. Kim, C. Kurdak, J. W. Allen, K. Sun, X. H. Chen, Y. Y. Wang, Z. Fisk, and L. Li, Two-dimensional Fermi surfaces in Kondo insulator SmB_6 , *Science* **346**, 1208 (2014).
- [32] Z. Xiang, B. Lawson, T. Asaba, C. Tinsman, L. Chen, C. Shang, X. H. Chen, and L. Li, Bulk Rotational Symmetry Breaking in Kondo Insulator SmB_6 , *Phys. Rev. X* **7**, 031054 (2017).
- [33] B. S. Tan, Y.-T. Hsu, B. Zeng, M. C. Hatnean, N. Harrison, Z. Zhu, M. Hartstein, M. Kiourlappou, A. Srivastava, M. D. Johannes, T. P. Murphy, J.-H. Park, L. Balicas, G. G. Lonzarich, G. Balakrishnan, and S. E. Sebastian, Unconventional Fermi surface in an insulating state, *Science* **349**, 287 (2015).
- [34] M. Hartstein, W. Toews, Y.-T. Hsu, B. Zeng, X. Chen, M. Hatnean, Q. Zhang, S. Nakamura, A. Padgett, G. Rodway-Gant, J. Berk, M. Kingston, G. Zhang, M. Chan, S. Yamashita, T. Sakakibara, Y. Takano, J.-H. Park, L. Balicas, N. Harrison, N. Shitsevalova, G. Balakrishnan, G. Lonzarich, R. Hill, M. Sutherland, and S. Sebastian, Fermi surface in the absence of a Fermi liquid in the Kondo insulator SmB_6 , *Nature Phys.* **14**, 166 (2018).
- [35] M. Hartstein, H. Liu, Y.-T. Hsu, B. Tan, M. Hatnean, G. Balakrishnan, and S. Sebastian, Intrinsic Bulk Quantum Oscillations in a Bulk Unconventional Insulator SmB_6 , *iScience* **23**, 11 (2020).
- [36] D. Chowdhury, I. Sodemann, and T. Senthil, Mixed-valence insulators with neutral Fermi surfaces, *Nature Comm.* **9**, 1766 (2018).
- [37] Y. Xu, S. Cui, J. K. Dong, D. Zhao, T. Wu, X. H. Chen, K. Sun, H. Yao, and S. Y. Li, Bulk Fermi Surface of Charge-Neutral Excitations in SmB_6 or Not: A Heat-Transport Study, *Phys. Rev. Lett.* **116**, 246403 (2016).
- [38] O. Erten, P.-Y. Chang, P. Coleman, and A. M. Tsvelik, Skyrme Insulators: Insulators at the Brink of Superconductivity, *Phys. Rev. Lett.* **119**, 057603 (2017).
- [39] J. Knolle and N. R. Cooper, Quantum Oscillations without a Fermi Surface and the Anomalous de Haas-van Alphen Effect, *Phys. Rev. Lett.* **115**, 146401 (2015).
- [40] P. Hlawenka, K. Siemensmeyer, E. Weschke, A. Varykhalov, J. Sanchez-Barriga, N. Y. Shitsevalova, A. Dukhnenko, V. Filipov, S. Gabani, K. Flachbart, O. Rader, and E. Rienks, Samarium hexaboride is a trivial surface conductor, *Nature Comm.* **9**, 517 (2018).
- [41] Y. S. Eo, S. Wolgast, A. Rakoski, D. Mihaliov, B. Y. Kang, M. S. Song, B. K. Cho, M. C. Hatnean, G. Balakrishnan, Z. Fisk, S. R. Saha, X. Wang, J. Paglione, and C. Kurdak, Comprehensive surface magnetotransport study of SmB_6 , *Phys. Rev. B* **101**, 155109 (2020).
- [42] C. E. Matt, H. Pirie, A. Soumyanarayanan, Y. He, M. M.

- Yee, P. Chen, Y. Liu, D. T. Larson, W. S. Paz, J. J. Palacios, M. H. Hamidian, and J. E. Hoffman, Consistency between ARPES and STM measurements on SmB_6 , *Phys. Rev. B* **101**, 085142 (2020).
- [43] S. M. Thomas, X. Ding, F. Ronning, V. Zapf, J. D. Thompson, Z. Fisk, J. Xia, and P. F. S. Rosa, Quantum Oscillations in Flux-Grown SmB_6 with Embedded Aluminum, *Phys. Rev. Lett.* **122**, 166401 (2019).
- [44] Y. S. Eo, K. Sun, C. Kurdak, D.-J. Kim, and Z. Fisk, Inverted Resistance Measurements as a Method for Characterizing the Bulk and Surface Conductivities of Three-Dimensional Topological Insulators, *Phys. Rev. Applied* **9**, 044006 (2018).
- [45] Y. Eo, A. Rakoski, J. Lucien, D. Mihaliov, C. Kurdak, P. Rosa, and Z. Fisk, Transport gap in SmB_6 protected against disorder, *Proc. Nat. Ac. Sci.* **116**, 26 (2019).
- [46] Y. S. Eo, A. Rakoski, S. Sinha, D. Mihaliov, W. T. Fuhrman, S. R. Saha, P. F. S. Rosa, Z. Fisk, M. C. Hatanen, G. Balakrishnan, J. R. Chamorro, W. A. Phelan, S. M. Koohpayeh, T. M. McQueen, B. Kang, M.-s. Song, B. Cho, M. S. Fuhrer, J. Paglione, and C. Kurdak, Bulk transport paths through defects in floating zone and Al flux grown SmB_6 , *Phys. Rev. Materials* **5**, 055001 (2021).
- [47] L. Jiao, S. Robler, D. Kasinathan, P. F. S. Rosa, C. Guo, H. Yuan, C.-X. Liu, Z. Fisk, F. Steglich, and S. Wirth, Magnetic and defect probes of the Sm_6 surface state, *Science Advances* **4** (2018).
- [48] J. C. Souza, P. F. S. Rosa, J. Sichelschmidt, M. Carlone, P. A. Venegas, M. O. Malcolms, P. M. Menegasso, R. R. Urbano, Z. Fisk, and P. G. Pagliuso, Metallic islands in the Kondo insulator SmB_6 , *Phys. Rev. Research* **2**, 043181 (2020).
- [49] N. J. Laurita, C. M. Morris, S. M. Koohpayeh, P. F. S. Rosa, W. A. Phelan, Z. Fisk, T. M. McQueen, and N. P. Armitage, Anomalous three-dimensional bulk ac conduction within the Kondo gap of SmB_6 single crystals, *Phys. Rev. B* **94**, 165154 (2016).
- [50] N. Laurita, C. Morris, S. Koohpayeh, W. Phelan, T. McQueen, and N. Armitage, Impurities or a neutral Fermi surface? A further examination of the low-energy ac optical conductivity of SmB_6 , *Physica B: Condensed Matter* **536**, 78 (2018).
- [51] S. Lee, V. Stanev, X. Zhang, D. Stasak, J. Flowers, J. Higgins, S. Dai, T. Blum, X. Pan, V. Yakovenko, J. Paglione, R. Greene, V. Galitski, and I. Takeuchi, Perfect Andreev reflection due to the Klein paradox in a topological superconducting state, *Nature* **570**, 344 (2019).
- [52] S. Bae, S. Lee, X. Zhang, I. Takeuchi, and S. M. Anlage, Microwave Meissner screening properties of proximity-coupled topological-insulator / superconductor bilayers, *Phys. Rev. Materials* **3**, 124803 (2019).
- [53] W. Phelan, S. Koohpayeh, P. Cottingham, J. Tutmaher, J. Leiner, M. Lumsden, C. Lavelle, X. Wang, C. Hoffmann, M. Siegler, N. Haldolaarachchige, D. Young, and T. McQueen, On the Chemistry and Physical Properties of Flux and Floating Zone Grown SmB_6 Single Crystals, *Sci. Reps.* **6**, 20860 (2016).
- [54] L. Fu and C. L. Kane, Superconducting Proximity Effect and Majorana Fermions at the Surface of a Topological Insulator, *Phys. Rev. Lett.* **100**, 096407 (2008).
- [55] M. C. Nuss and J. Orenstein, Terahertz time-domain spectroscopy, in *Millimeter and Submillimeter Wave Spectroscopy of Solids*, edited by G. Grüner (Springer Berlin Heidelberg, Berlin, Heidelberg, 1998) pp. 7–50.
- [56] D. C. Mattis and J. Bardeen, Theory of the Anomalous Skin Effect in Normal and Superconducting Metals, *Phys. Rev.* **111**, 412 (1958).
- [57] M. Dressel and G. Gruner, *Electrodynamics of Solids: Optical Properties of Electrons in Matter* (Cambridge University Press, 2002).
- [58] M. Tinkham, *Introduction of Superconductivity, 2nd Ed.* (Dover Publications, 2004).
- [59] P. de Gennes, Boundary Effects in Superconductors, *Rev. Mod. Phys.* **36**, 225 (1964).
- [60] J. Clarke, The Proximity Effect Between Superconducting and Normal Thin Films in Zero Field, *Journal de Physique Colloques* **29**, C2 (1968).
- [61] P. Chauhan, F. Mahmood, D. Yue, P.-C. Xu, X. Jin, and N. P. Armitage, Nodeless Bulk Superconductivity in the Time-Reversal Symmetry Breaking Bi/Ni Bilayer System, *Phys. Rev. Lett.* **122**, 017002 (2019).
- [62] N. Koirala, M. Brahlek, M. Salehi, L. Wu, J. Dai, J. Waugh, T. Nummy, M.-G. Han, J. Moon, Y. Zhu, D. Dessau, W. Wu, N. P. Armitage, and S. Oh, Record Surface State Mobility and Quantum Hall Effect in Topological Insulator Thin Films via Interface Engineering, *Nano Letters* **15**, 8245 (2015).
- [63] L. Wu, W.-K. Tse, M. Brahlek, C. M. Morris, R. V. Aguilar, N. Koirala, S. Oh, and N. P. Armitage, High-Resolution Faraday Rotation and Electron-Phonon Coupling in Surface States of the Bulk-Insulating Topological Insulator $\text{Cu}_{0.02}\text{Bi}_2\text{Se}_3$, *Phys. Rev. Lett.* **115**, 217602 (2015).
- [64] L. Wu, M. Salehi, N. Koirala, J. Moon, S. Oh, and N. P. Armitage, Quantized Faraday and Kerr rotation and axion electrodynamics of a 3D topological insulator, *Science* **354**, 1124 (2016).
- [65] Y. Jiang, M. M. Asmar, X. Han, M. Ozerov, D. Smirnov, M. Salehi, S. Oh, Z. Jiang, W.-K. Tse, and L. Wu, Electron-Hole Asymmetry of Surface States in Topological Insulator Sb_2Te_3 Thin Films Revealed by Magneto-Infrared Spectroscopy, *Nano Letters* **20**, 4588 (2020).